IEEE Access
Multidisciplinary | Rapid Review | Open Access Journal

Received 26 February 2023, accepted 18 March 2023, date of publication 27 March 2023, date of current version 6 April 2023.

Digital Object Identifier 10.1109/ACCESS.2023.3262465

RESEARCH ARTICLE

An EEG-Based Brain-Computer Interface Using Spectral Correlation Function

NAZILA PANAHI, MEHDI CHEHEL AMIRANI, AND MORTEZA VALIZADEH
Department of Electrical Engineering, Urmia University, Urmia 5756151818, Iran
Corresponding author: Morteza Valizadeh (mo.valizadeh@urmia.ac.ir)

ABSTRACT Brain-Computer Interface (BCI) is a promising technique because of its wide variety of applications, from treating cognition in humans to person authentication. Brain signals can be transmitted straight to a prosthetic device from the BCI system, without the need for nerve or muscle activity. For accurately identifying the transmitted signals at the prosthetic device, considering the nature of the Electroencephalography (EEG) signal, and extracting the most informative features are effective keys. In this paper, we studied the cyclostationarity of the Slow Cortical Potential (SCP) EEG signals for BCI applications, following our previous studies. Cyclostationary analysis reveals the hidden periodicity in the signal and provides a second-order statistical description in the frequency domain. We used the FFT Accumulation Method (FAM), an effective computational algorithm, to extract the features of the Spectral Correlation Function (SCF). The features are classified using SVM RBF, SVM polynomial, and K-Nearest Neighbor classifiers, and they are considered with different pre-processing. Our research indicates that the SCP EEG signal has cyclostationary properties and this idea is applied to the BCIs as well. The classification accuracy on the BCI Competition 2003 dataset Ia's increased considerably, by spotting the intrinsic correlation between just two EEG signals.

INDEX TERMS Brain-computer interface (BCI), cyclostationary signal, spectral correlation function (SCF), electroencephalography (EEG) classification, BCI competition 2003 dataset Ia.

I. INTRODUCTION

Research on the Brain-Computer Interface (BCI) began at the University of California (UCLA) in the 1970s with animal studies on how to build a direct link between external environments (or gadgets) and the brain; the first human attempts came in the 1990s [1]. Technologies based on BCIs were created to assist people who have problems interacting with their surroundings. In this application, brain signals are directly transmitted from the BCI system to an external device, such as a robotic arm, prosthetic device, or wheelchair, without needing healthy or fully functional nerves and muscles. The brain impulses used for computer-brain communication have advanced from feelings and perceptions to higher levels of thought with an improvement of neurotechnology and artificial intelligence, transforming BCIs into a new generation of hybrid intelligence known as Brain-computer intelligence [2]. Human information processing, decision-making, and perceptual skills can be enhanced by the collaboration of Human Intelligence (HI) with Artificial Intelligence (AI) in non-medical applications [3], [4], [5], [6], [7].

A BCI system goes through six basic processing phases: data collecting, background noise removal, application-specific feature extraction, selection of the most important features, classification of the collected features to make decisions, and delivering control commands to an end machine, carrying out the orders, and providing feedback to the user by machine. BCIs may not always use feature-selection and feedback-sending techniques to minimize computations, but those that look for salient features increase accuracy [8]. In particular, the preprocessing, feature extraction, and classification phases were the focus of many research efforts to enhance their performance [9], [10], [11], [12], [13], [14], [15], [16], [17], [18], [19], [20].

Brain imaging data is collected while the person performs an imaginary action, such as moving a hand, arm, tongue,

The associate editor coordinating the review of this manuscript and approving it for publication was Md. Kafiul Islam.

TABLE 1. Neuroimaging approaches comparison.

Method	Activity Measured	Risk	Spatial Resolution	Temporal Resolution
EEG	Electrical	Non- invasive	~ 10 mm	~ 0.001 s
ECoG	Electrical	Semi- invasive	~ 1 mm	~ 0.003 s
MEG	Magnetic	Non- invasive	~ 5 mm	~ 0.05 s
PET	Metabolic	Non- invasive	~ 1 mm	~ 0.2 s
fMRI	Metabolic	Non- invasive	~ 1 mm	~ 1 s
NIRS	Metabolic	Non- invasive	~ 2 cm	~ 1 s

A comparison of the mentioned neuroimaging approaches [22].

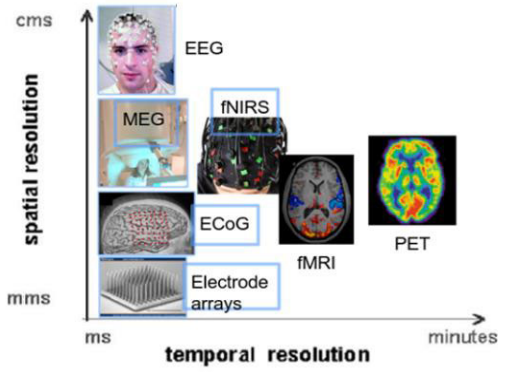

FIGURE 1. Comparison of the temporal and spatial resolution for various neuroimaging approaches [28].

or leg, tracking the movement of an imaging cursor, etc. By analyzing these signals, we can distinguish different types of mental tasks. The information can be gathered using a variety of methods: 1) Functional Magnetic Resonance Imaging (fMRI) [21], Positron Emission Tomography (PET) [22], and Near-Infrared Spectroscopy (NIRS) [23], all of which measure changes in the brain blood flow; 2) Magnetoencephalography (MEG) [24] which measures the brain's magnetic activity; 3) Electroencephalography (EEG) [11] and Electrocorticography (ECoG) [25] which measure the brain's electrical activity; 4) Hybrid BCI (hBCI) [26], [27] which combines the above-mentioned methods. MEG and fMRI are currently prohibitively expensive, and PET necessitates a radioactive injection, so NIRS and EEG are more widely utilized signals [28]. Temporal resolution detects brain activity in real time, whereas spatial resolution indicates the specific position of the action. MEG and PET's temporal and spatial resolutions are high, fMRI and NIRS are low, and EEG has a high temporal but low spatial resolution. A comparison of the mentioned neuroimaging approaches is shown in table 1 [22] and figure 1 [28].

Electroencephalography (EEG) is a non-invasive technique for collecting brain electrical activity. Typically, EEG electrodes are placed on the scalp surface in a 10–20 global deployment pattern as shown in figure 2 [7]. Each electrode records a one-dimensional vector of raw EEG data as the signals are recorded on the three-dimensional scalp surface. The EEG data is noisy due to hair, fatty tissue, and eye blinking. In addition, artifacts could be created by the recording equipment's power connections and electrode movement.

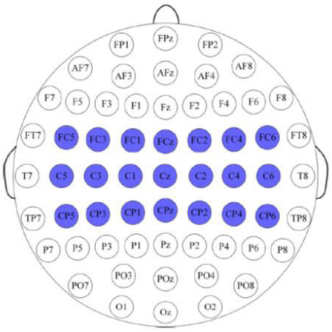

FIGURE 2. EEG electrode placement according to the 10-20 system. The related motor imagery (MI) electrodes are identified in blue color [7].

Consequently, a large amount of weak and low signal-to-noise ratio data is recorded. As a result, signal classification and interpretation get more difficult. Despite its drawbacks, raw EEG has certain benefits over other brain imaging methods, such as low cost, portability, and the lack of side effects because it is non-invasive. Hence, EEG offers many applications, including screening and hypothesis-based diagnosis such as diagnosis of depression [29], Alzheimer's [30], epileptic seizures [31], neuromarketing [32], neuro-entertainment [33], [34], borderline personality disorder [35], sleep stage classification [36], robot-assisted therapy [37], wheelchair control [38], person identification and authentication [39], [40], [41], social interaction [42], speech BCIs [43], [44], [45], [46], driver drowsiness detection [47], and so on.

Assistive studies typically use EEG data from the motor cortex region, whose electrodes are indicated in blue in figure 2 [7]. Researchers studying BCIs are interested in EEG signals such as Slow Cortical Potentials (SCP) [11], [12], [13], [14], [15], [16], [17], [18], [19], [20], [48], [49], Steady-State Visual Evoked Potentials (SSVEP) [50], [51], motion onset Visual Evoked Potential (moVEP) [52], P300 [53], [54], [55], and others.

The classification of Slow Cortical Potential (SCP) signals is crucial not only for BCI but also for several other disciplines, including stroke rehabilitation [56] and neuroscience research [57], [58], [59]. Furthermore, SCP signals are strongly correlated with Attention Deficit Hyperactivity Disorder (ADHD) [60], [61], [62], and numerous studies have shown that teaching patients to modify their SCP signals dramatically raises their test results for behavior, focus, and Intelligence Quotient (IQ) [63].

Extracting application-specific features is an important step in BCIs, and a variety of features have been proposed to improve classification accuracy. For accurate detection of mental activity, the ability of the extracted features to discriminate between them is crucial. To achieve the highest degree of accuracy, several features must be combined in most cases. The BCI competition II dataset Ia [64], detailed in Section II, is a commonly used dataset for SCP EEG signals, and here's a brief overview of the studies that have been published using it:

Mensh et al. [48], the 2003 BCI competition winners, looked at the time-domain and frequency-domain averages for six EEG channels and used four features in their classification algorithm based on the statistical significance between each trial of two classes. The features were the SCP amplitude of channels 1 and 2 as time-domain analysis, and the Gamma-band powers of channels 4 and 6 as frequency-domain analysis. The results of five classifiers are presented, with the best Correct Classification Rate (CCR) of 88.70% for SCP plus multi-taper classification.

Sun et al. [13] looked at the possibility of classifying EEG signals using common low-level features in audio/speech signal processing. Seven low-level features were generated from each 0.5 seconds subframe of six channels, and the most efficient features were selected by averaging the CCR for each channel and per each feature on the training set. It resulted in a CCR of 90.44%, obtained by fusing the selected features with DC potentials.

Wang et al. [65] proposed a method with Wavelet Packet Transform (WPT) and Artificial Neural Networks (ANNs). Using wavelet packets, SCPs are combined with the energy of the time-frequency domain in the beta-band. The classification consists of a three-layer perceptron established by Back-Propagation (BP) and Support Vector Machines (SVMs) for channels 1 and 2. The best classification accuracy was 91.47% for the BP network.

Li et al. [14] studied the EEG classification by chaos theory. As EEG is a complex time series that behaves like an unstable unusual attractor in a chaotic system rather than a random signal [66], the chaos theory may provide helpful quantitative descriptions. Because the complexity measures may characterize the complexity of a chaotic system, two additional characteristics are presented to analyze EEG signals in the BCI system: Kolmogorov and C0 complexity measures. The success rate of the experiment was 90.3% CCR using the two most important channels (channels 1 and 2).

Approaches based on polynomial fitting coefficients were proposed by Kayikcioglu et al. [15] and Hou et al. [19]. The coefficients of a second-order polynomial fitted to just one EEG channel (channel 1) produced the feature vector in [15]. Still, the simulation results for two channels (channels 1 and 2) are also shown. The K-Nearest Neighbor (KNN), Multiple Layer Perceptron (MLP), and Support Vector Machine (SVM) algorithms are used to assess the performance of the extracted features. The best outcome for one-channel processing and the KNN classifier is 92.15% CCR. The method presented in [19] extracts the features by fitting a second-order polynomial to the wavelet coefficients of SCP signals. Then, a voting system based on the optimal training parameters of the SVM (VSVM) enhances the classification accuracy. In this algorithm, the best CCR for just one EEG channel (channel 1) is 94.50%.

Wavelet Packet Decomposition (WPD) is used by Hu et al. [16] to extract features. The wavelet packet decomposition means that the energy of a specific sub-bands serves as the coefficients. Using Fisher Discriminant Analysis (FDA), the separable features are selected. The chosen features from the six channels are then combined to form the feature vector. The K-Nearest Neighbor (KNN) algorithm is then used to classify the attributes. This study's CCR is 90.10%.

Duan et al. [17] extracted features using Linear Discriminate Analysis (LDA) and Principal Component Analysis (PCA). According to their earlier research [67], only signals from channels 1 and 2 are utilized. The raw data was divided into nine sections. Each segment is linked to PCA, and the optimal data string is chosen based on a 99% Accumulative Contribution Rate (ACR). LDA then processes the features, and the classification is carried out by a Voting-based Extreme Learning Machine (V-ELM). The accuracy of the classification is 93.52%.

Nguyen et al. apply wavelet coefficients [18]. This technique combines wavelet modification with an Interval Type-2 Fuzzy Logic System (IT2FLS). The most valuable coefficients are inputs to the IT2FLS for the classification step after wavelet coefficients are sorted according to the statistics of the receiver operating characteristic curve criterion. Feedforward neural networks, SVMs, k-nearest neighbors, AdaBoost, and adaptive neuro-fuzzy classifiers are used for comparisons. The highest rating, 90.10%, belongs to IT2FLS.

PCA and LDA are combined by Duan et al. [20] to extract features. The first step is to utilize the PCA algorithm to minimize the data's dimension. Then, after determining the best projection direction for channels 1 and 2, LDA is used to produce a collection of projective feature vectors for the training samples that have the biggest between-class scatter and the least within-class scatter. After that, the Multilayer Extreme Learning Machine (ML-ELM) classifies the features. A 94.20% performance rating has been given.

Log Energy Entropy of wavelet packet analysis was used by Göksu [68] to create the features. The feature vectors are fed into a Multilayer Perceptron (MLP) classifier, and the MLP's performance is compared to that of the KNN and SVM classifiers. The approach delivers 92.8% accuracy.

Paranjape et al. [11] investigated the feature extracted by correlating EEG data with SCP of the most efficient channels (channels 1 and 2) via a cross-correlation approach. First, the reference signal is chosen according to a criterion rather than the randomly chosen ways. After that, the discriminative characteristics are obtained from each cross-correlated sequence. Peak value, peak value number, centroid, equivalent width, and mean square abscissa construct feature vectors, then classified using SVM and KNN classifiers. The authors recommended creating an ensemble of SVM classifiers trained with complementary feature sets to improve classification accuracy. The highest score is 94.54%.

The categorization methods created by Annaby et al. [12] are based on graph-theoretic models. A directed graph of the EEG channels is connected by multivariate autoregressive models. Additionally, Gaussian-weighted distances between

graph nodes are used to build models of undirected graph signals. The Fourier transform is then applied to a new graph iteration between the directed and undirected graph models. The transform coefficients are used to extract the distinctive features. Also, to improve the discriminative power of features, the principal components, comparable spatial patterns, and polynomial representations were applied. Extreme Learning Machine (ELM) classifiers significantly improved their performance and produced a classifier with an accuracy of 96.58% using fully connected and weighted directed graph features computed on delta-.band EEG data.

Although various BCI algorithms have been examined, research on efficient feature extraction by considering the essence of EEG signals is still ongoing. According to Kumar et al. [69], the almost constant presence of non-stationarities in EEG signals degrades BCI performance. In an information theoretic context, the authors suggested a novel strategy based on Joint Approximate Diagonalization (JAD) to optimize stationarity for multiclass motor imagery BCIs. In particular, they estimate the subspace in the suggested manner that maximizes the discriminability between classes while simultaneously maintaining stationarity within the classes. On an orthogonal manifold, they use gradient descent optimization to find the subspace for the suggested technique. Results on BCI competition IV dataset IIa indicate an improvement in the average classification accuracy over the baseline methods, which is crucial for reducing non-stationarities within sessions.

As pointed out by Sadatnejad et al. [70], in the current BCI systems, between-session non-stationarity poses a significant performance issue. They investigated the application of the channel selection technique with Riemannian BCI classifiers to reduce between-session non-stationarity. To exclude the least significant channels, a sequential floating backward selection search method was used. The suggested methods were evaluated using three multi-session and multi-class Mental Tasks based (MT-based) BCI datasets. They obtained noticeable performance enhancements compared to using all channels. They concluded that Riemannian BCI classification accuracy could be significantly increased by reducing non-stationarity through channel selection.

Some phenomena, such as brain and heart activity, are incapable of being formulated. The cyclostationarity hypothesis of the EEG and Electrocardiogram (ECG) signals cannot currently be proven; but intuitively it can be understood, even though it is not clear, and that is why such periodicity is called hidden periodicity. We investigated this theory, and the findings support it. In this study, we investigated the cyclostationarity of the Slow Cortical Potentials (SCP) EEG signals, following our previous studies on ECG [71] and EEG [72] signals. Cyclostationary signals are continuous random signals that undergo periodic changes in their statistical features across time [73]. The Spectral Correlation Function (SCF), which is the cross-spectral of a signal and its frequency-shifted version, produces a second-order statistical representation of the signal in the frequency domain. The SCF is also referred to as the cyclic spectrum, and the theory behind it is covered in references [74], [75], [76]. The fundamentals of time and frequency smoothing methods are the same in spectral correlation analysis [73], [77]. The Strip Spectral Correlation Analyzer (SSCA) and the FFT Accumulation Method (FAM), are two time smoothing techniques that utilize the computation efficiency of FFT. They were both developed in [76] and discussed in [78]. The effectiveness of cyclostationary analysis has been tested in several disciplines. Amirani et al. [79] demonstrated that modulation classification based on cyclic spectrum analysis performs well, and [80] and [81] showed that this concept could also be applied to texture classification. Each image provides two one-dimensional signals by sorting pixels row by row and column by column. The SCF of each signal is then calculated using the FAM. According to the results of the experiments, the suggested method improves the retrieval accuracy, and the CCR of the recovered features is more distinct compared to typical discrete wavelet transform techniques. Mihandoost et al. [71] and [72] presented the SCF analysis as a feature extraction approach for ECG representation and epilepsy diagnosis, respectively. The authors use FAM for SCF calculation and also employ a statistical model called Generalized Autoregressive Conditional Heteroscedasticity (GARCH), as a describing model by taking into account the heteroscedastic quality of SCF coefficients, and also to decrease the number of features. The experimental findings show that the proposed approach is effective.

We investigated the cyclostationarity of the Slow Cortical Potentials (SCP) EEG signals and our studies suggest that BCIs can also benefit from this concept. The SCF takes advantage of the nature of EEG as well as current BCI research problems including optimum feature selection and multiple-channel processing. The proposed method was evaluated on the BCI Competition 2003 dataset Ia and the results showed that it can classify the EEG signals for BCIs applications precisely. Additionally, considering the aforementioned works [12], [17], [20] and also our earlier article [82], we investigated the effects of feature preprocessing using PCA and LDA techniques.

The rest of this paper is organized as follows. In Section II, the employed EEG dataset is briefly described. Section III discusses the SCF and FFT accumulation methods. In Section IV, the experimental setup and results are presented. Section V concludes with research suggestions for the future.

II. DATASET

The EEG recordings submitted for dataset Ia of the BCI Competition 2003 were made by a healthy subject [64]. A1-Cz, A2-Cz, 2 cm frontal of C3, 2 cm parietal of C3, 2 cm frontal of C4, and 2 cm parietal of C4 were the six locations where EEG data were recorded, as shown in figure 3 (a). The subject was asked to move the cursor on the computer screen while

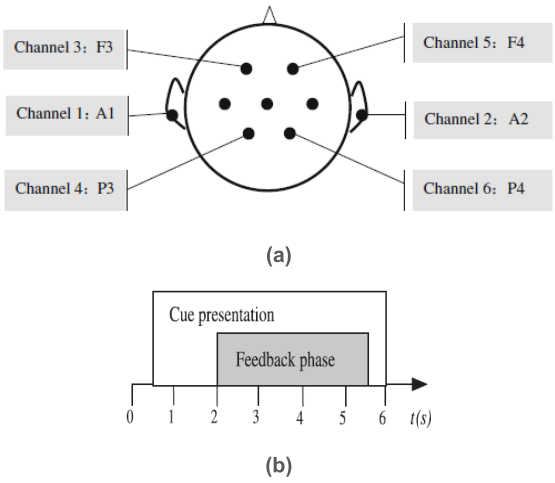

FIGURE 3. (a) The six locations where EEG electrodes [17] and (b) the layout of the trial [11].

his cortical potentials were being measured. Each reading is expressed in microvolts. The recording gave the subject visual feedback on his slow cortical potential. Depending on whether the cortical state is positive or negative, the pointer on the screen oscillates between lower and higher positions. Each trial lasted six seconds. In each trial, a target was highlighted at the top or bottom of the screen to represent negativity (Class 0) or positivity (Class 1), respectively. After 0.5 seconds, the stimulation began, and it lasted until the trial was complete. With a 256 Hz sampling rate and a 3.5 s recording time, 896 samples per channel were taken from each trial. Figure 3 (b) depicts the layout of the trial. The 268 trials for the training dataset, 135 of which were in Class 0 and 133 of which were in Class 1, were recorded and tagged over two distinct days and then mixed randomly. For the test dataset on the second day, 293 trials were recorded, including 147 trials for Class 0 and 146 trials for Class 1. The vertical eye movement artifacts were removed from the SCP measurements, according to [83].

III. SPECTRAL CORRELATION FUNCTION

For a discrete-time real-valued signal $x(n)$, the cyclic autocorrelation is defined by [73]:

$$R_x^{\alpha}(k) = \lim_{N\to\infty} \frac{1}{2N+1} \sum_{n=-N}^{N} [x(n+k)e^{-j\pi\alpha(n+k)}][x(n)e^{j\pi\alpha n}]^* \tag{1}$$

the Fourier transform of the cyclic autocorrelation function,

$$S_x^{\alpha}(f) = \sum_{n=-\infty}^{\infty} R_x^{\alpha}(k)e^{-j2\pi fk} \tag{2}$$

is called the Spectral Correlation Function (SCF). Since the multiplication of a signal by $e^{\pm j\pi\alpha n}$ shifts the spectral content of the signal by $\pm\alpha/2$, the cross-spectrum of the pair of complex-valued frequency-shifted signals $x(n)e^{-j\pi\alpha n}$ and $x(n)e^{j\pi\alpha n}$ provides a suitable interpretation of the SCF. In this explanation, the parameter α, called the cyclic frequency, is the relative frequency shift and f is the cross spectrum frequency variable. The number of alpha values or $S_x^{\alpha}(f) \neq 0$ is countable if the signal has finite average power [74]. The ordinary power spectrum is obtained by $\alpha = 0$, as:

$$S_x(f) = S_x^0(f) = \sum_k R_x^0(k)e^{-j2\pi fk} \tag{3}$$

Clearly, the SCF offers more comprehensive features regarding ordinary power spectral density. Two inherent properties of SCF for real-valued signals indicate that the entire function is determined by $\{0 \le f \le 1/2, 0 \le \alpha \le 1 - 2f\}$, where f is the normalized frequency. The first property is symmetry relationships $S_x^{\alpha}(-f) = S_x^{\alpha}(f)$ and $S_x^{-\alpha}(-f) = S_x^{\alpha}(f)^*$ and the second is periodicity associated with discrete-time for any integer m and n, $S_x^{\alpha+n}(f + m + n/2) = S_x^{\alpha}(f)$. These qualities can be easily proved using the definition of SCF.

Several computationally efficient cyclic spectral analysis algorithms have been proposed, which are categorized by average frequency (frequency smoothing methods) or average time (time smoothing methods). The FFT Accumulation Method (FAM) algorithm, belonging to the time smoothing category, is used in this article. Therefore, we only explain the fundamentals of time smoothing algorithms, and the more extensive discussion can be found in [73]. The all-time smoothing procedures are based on the time smoothed cyclic cross periodogram [75]:

$$S_{x_T}^{\alpha}(n,f)_{\Delta T} = \frac{1}{T}\left\langle X_T\left(n, f+\alpha/2\right), X_T^*\left(n, f-\alpha/2\right)\right\rangle_{\Delta T} \tag{4}$$

The correlation of spectral components of $x(n)$ over a time span of Δt seconds is the physical interpretation of the time smoothed cyclic periodogram. The complex envelopes of narrow-band, bandpass components of a signal, called complex demodulates, are represented by the spectral components $X_T\left(n, f+\alpha/2\right)$ and $X_T^*\left(n, f-\alpha/2\right)$. A data tapering window of length T slides over the data for a period of Δt to calculate the $S_{x_T}^{\alpha}(n,f)_{\Delta T}$. The complex demodulation of the data within the window are calculated at each instant. Then, by time-averaging conjugate products for Δt seconds, the correlation is done, and the estimates of the cyclic spectrum function are obtained. The correlation of demodulates separated in the frequency domain by the amount α_0 and centered on a midpoint of f_0 is used to estimate the cyclic spectrum at the point (f_0, α_0). The point estimate's time and frequency resolutions are denoted by the quantities Δt and Δf, respectively.

$$X_T(n,f) = \sum_{n=-N'/2}^{N'/2} a(r)x(n-r)e^{-j2\pi f(n-r)T_s} \tag{5}$$

where $a(r)$ is a data tapering window of length $T = N'T_s$. The complex demodulates then correlated over a Δt seconds

time span:

$$S_{x_T}^{\alpha_0}(n,f_0)_{\Delta t} = \sum_r X_T(r,f_1)X_T^*(r,f_2)g(n-r) \quad (6)$$

where $g(n)$ is a data tapering window of width $\Delta t = NT_s$, $f_1 = f_0 + \alpha_0/2$ and $f_2 = f_0 - \alpha_0/2$. The time-smoothed cyclic cross periodogram converges to the cyclic cross-spectrum if the time windows $a(n)$ and $g(n)$ are appropriately normalized, as $\Delta t \to \infty$ followed by $\Delta f \to 0$, [84]. Therefore, if $\sum a^2(n) = \sum g(n) = 1$, then

$$\lim_{\Delta f \to 0} \lim_{\Delta t \to \infty} S_{X_T}^{\alpha_0}(n,f_0)_{\Delta t} = S_X^{\alpha_0}(f_0) \quad (7)$$

The Fourier transform is used to smooth time in the FAM algorithm. If the frequency is shifted from α_0 to $\alpha_0 + \varepsilon$, the output of the system is provided by:

$$S_{X_T}^{\alpha_0+\varepsilon}(n,f_0)_{\Delta t} = \sum_r X_T(r,f_1)X_T^*(r,f_2)g(n-r)e^{-j2\pi\varepsilon r T_s} \quad (8)$$

by discretizing the value of the script ε to $\varepsilon = q\Delta\alpha$, the sum evaluation can be simplified. So, the algorithm's result is stated as:

$$S_{X_T}^{\alpha_0+q\Delta\alpha}(n,f_j)_{\Delta t} = \sum_r X_T(r,f_1)X_T^*(r,f_2)g(n-r)e^{-j2\pi rq/N} \quad (9)$$

This expression evaluates the sum with an N-point FFT. Fourier, transforms the product sequences instead of averaging them separately; point estimates with constant cycle frequency can be obtained in blocks, which increases the algorithm's speed. A bank of bandpass filters is required to cover the bi-frequency plane and generate the necessary complex demodulates. An efficient method based on a sliding FFT [85] can be used. The frequencies of the filter bank are discretized in this method to:

$$f_k = k\left(f_s/N'\right), k = -N'/2, \ldots, N'/2 - 1 \quad (10)$$

An SCF estimation is located at the frequencies, and cycle frequencies associated with the complex demodulates (f_j, α_i):

$$f_j = (f_k + f_l)/2 = (k+l)(f_s/N')/2 \quad (11)$$

$$\alpha_i = f_k - f_l = (k-l)(f_s/N') \quad (12)$$

A N'-point channelizer can have $(N')^2$ possible combinations of channelizer streams; thus, there is at most $(N')^2$ estimation region (diamond region). Because of symmetry, only $(N')^2/4$ diamond areas are required to estimate the cyclic spectrum of a real signal (one quadrant of the bi-frequency plane).

1- Four reference signals are chosen to represent the classes "up" and "down" of two channels, similarly to [11]. The reference signal is the signal whose mean and standard deviation values are closest to the class averages.

IV. THE EXPERIMENTAL SETUP AND RESULTS

Finding the most similarity between data from the same class or the most dissimilarity between data from different classes, or both, is necessary to solve classification problems successfully. In this research, we studied the applicability of the Spectral Correlation Function (SCF) in BCIs because it uncovers the hidden periodicity and intrinsic correlation between two signals. By changing the correlation algorithm in the feature extraction block, the performance of the methodology described in [11] was significantly enhanced.

TABLE 2. Feature packs.

Pack number	Containing Features
Pack 1	Peak value, equivalent width, mean square abscissa
Pack 2	Peak value, instant at which peak occurs, equivalent width, mean square abscissa
Pack 3	equivalent width, mean square abscissa
Pack 4	centroid, equivalent width, mean square abscissa
Pack 5	centroid, equivalent width

Different combinations of classification features

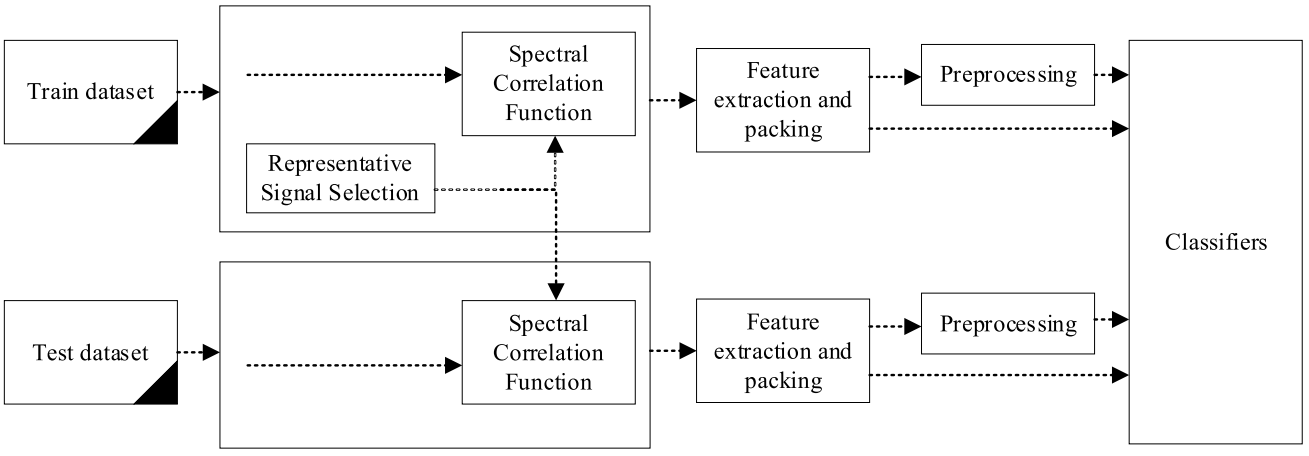

FIGURE 4. Flowchart of the proposed classification method.

TABLE 3. The classification accuracies for total features.

Data	Preprocessing / Classifier	SVM RBF	SVM POLYNOMIAL	KNN
Train dataset	not preprocessed	99.25	98.51	98.88
	PCA	99.25	98.88	98.69
	LDA	99.25	98.88	99.07
	LDA after PCA	99.44	98.88	99.07
	PCA after LDA	99.25	99.07	98.88
Train dataset	not preprocessed	99.83	99.66	99.83
	PCA	99.83	99.83	99.66
	LDA	99.83	99.83	99.83
	LDA after PCA	99.83	99.83	99.83
	PCA after LDA	99.83	99.66	99.66

The classification accuracies of the proposed approach for total features of the train and test datasets (not-preprocessed features).

TABLE 4. The classification accuracies per various feature packs.

Data	Feature Pack number / Classifier	SVM RBF	SVM POLYNOMIAL	KNN
Train dataset	Pack 1	99.44	99.44	98.69
	Pack 2	99.44	98.69	98.51
	Pack 3	65.30	51.12	68.10
	Pack 4	65.49	49.81	68.10
	Pack 5	55.78	50.19	55.60
Train dataset	Pack 1	99.83	99.83	99.83
	Pack 2	99.83	99.66	99.83
	Pack 3	87.03	59.04	86.52
	Pack 4	87.37	53.75	86.52
	Pack 5	57.85	51.19	58.53

The classification accuracies of the proposed approach for different feature packs of the train and test datasets (not-preprocessed features).

TABLE 5. The classification accuracies per various feature packs of the channel1 train dataset.

Data	Feature Pack / Classifier	SVM RBF	SVM POLYNOMIAL	KNN
not preprocessed	Pack 1	98.88	99.25	98.88
	Pack 2	99.25	99.25	98.88
	Pack 3	62.69	51.49	58.21
	Pack 4	63.06	45.52	58.21
	Pack 5	46.64	49.63	51.12
PCA preprocessed	Pack 1	97.76	99.63	94.78
	Pack 2	99.25	100	98.13
	Pack 3	43.66	52.24	50.37
	Pack 4	43.66	50.00	50.00
	Pack 5	45.90	45.90	51.12
LDA preprocessed	Pack 1	99.25	99.25	98.88
	Pack 2	98.88	99.25	98.88
	Pack 3	57.46	56.34	58.21
	Pack 4	47.39	48.88	50.00
	Pack 5	46.64	49.63	51.12
LDA after PCA preprocessed	Pack 1	99.25	99.63	99.63
	Pack 2	99.25	100	99.63
	Pack 3	43.66	52.99	50.37
	Pack 4	57.46	51.87	58.21
	Pack 5	45.90	46.27	51.12
PCA after LDA preprocessed	Pack 1	83.58	80.60	82.84
	Pack 2	98.13	98.88	94.78
	Pack 3	50.75	50.37	51.87
	Pack 4	42.91	52.61	48.88
	Pack 5	45.90	45.90	51.12

The classification accuracies of the proposed approach for each feature pack of the channel1 train dataset.

TABLE 6. The classification accuracies per various feature packs of the channel1 test dataset.

Data	Feature Pack / Classifier	SVM RBF	SVM POLYNOMIAL	KNN
not preprocessed	Pack 1	100	99.66	100
	Pack 2	100	99.66	100
	Pack 3	82.94	50.17	77.13
	Pack 4	82.94	55.29	77.13
	Pack 5	51.19	48.81	54.27
PCA preprocessed	Pack 1	91.81	100	95.56
	Pack 2	99.66	99.66	99.32
	Pack 3	47.44	55.32	55.29
	Pack 4	48.46	55.32	55.29
	Pack 5	50.17	47.10	54.27
LDA preprocessed	Pack 1	100	100	100
	Pack 2	100	99.66	100
	Pack 3	83.28	48.46	80.89
	Pack 4	55.63	49.15	59.04
	Pack 5	51.19	48.81	54.27
LDA after PCA preprocessed	Pack 1	100	100	100
	Pack 2	100	100	100
	Pack 3	47.44	53.79	55.29
	Pack 4	83.28	48.46	80.89
	Pack 5	50.17	47.10	54.27
PCA after LDA preprocessed	Pack 1	96.25	97.27	96.59
	Pack 2	100	99.66	100
	Pack 3	52.22	47.10	54.61
	Pack 4	47.10	53.92	54.95
	Pack 5	50.17	47.10	54.27

The classification accuracies of the proposed approach for each feature pack of the channel1 test dataset.

Only the data from channels 1 and 2 are used following [11] and considering previously published successful research. A description and flowchart of the suggested method and its outcomes are provided below. Classification steps are:

2- Correlated signals are produced by spectral correlating the reference and train/test signals.

3- The correlated signals are used to construct the five expressed features at [11]. The features are peak value, instant at which peak occurs, centroid, equivalent width, and mean square, as follows:

$$centroid = \frac{\sum_{l=-(N-1)}^{(N-1)} lC(l)}{\sum_{l=-(N-1)}^{(N-1)} C(l)} \tag{13}$$

$$euivalent\ width = \frac{\sum_{l=-(N-1)}^{(N-1)} C(l)}{peak\ value\ of\ C(l)} \tag{14}$$

$$mean\ square\ abscissa = \frac{\sum_{l=-(N-1)}^{(N-1)} l^2 C(l)}{\sum_{l=-(N-1)}^{(N-1)} C(l)} \tag{15}$$

where the variable l is the cross-spectrum frequency variable and $C(l)$ is the spectral-correlated signal.

4- As shown in table 2, features are packed in the five ways described in [11].

TABLE 7. The classification accuracies per various feature packs of the channel2 train dataset.

Data	Feature Pack / Classifier	SVM RBF	SVM POLYNOMIAL	KNN
not preprocessed	Pack 1	100	100	100
	Pack 2	100	100	97.76
	Pack 3	84.70	85.07	83.96
	Pack 4	84.70	85.45	83.96
	Pack 5	57.09	42.91	67.16
PCA preprocessed	Pack 1	100	100	100
	Pack 2	99.25	99.63	98.13
	Pack 3	62.31	33.21	66.42
	Pack 4	61.57	50.00	66.79
	Pack 5	56.72	51.49	67.16
LDA preprocessed	Pack 1	100	100	100
	Pack 2	100	100	98.13
	Pack 3	85.45	84.33	85.07
	Pack 4	75.00	51.49	72.76
	Pack 5	57.09	42.91	67.16
LDA after PCA preprocessed	Pack 1	100	100	100
	Pack 2	100	100	98.13
	Pack 3	62.31	33.21	66.42
	Pack 4	85.45	84.33	85.07
	Pack 5	56.72	51.49	67.16
PCA after LDA preprocessed	Pack 1	100	100	100
	Pack 2	99.25	100	98.13
	Pack 3	62.31	44.40	70.90
	Pack 4	82.09	79.85	80.22
	Pack 5	56.72	51.49	67.16

The classification accuracies of the proposed approach for each feature pack of the channel2 train dataset.

TABLE 8. The classification accuracies per various feature packs of the channel2 test dataset.

Data	Feature Pack / Classifier	SVM RBF	SVM POLYNOMIAL	KNN
not preprocessed	Pack 1	100	100	100
	Pack 2	100	100	100
	Pack 3	97.27	96.59	96.59
	Pack 4	97.27	96.93	96.59
	Pack 5	70.31	53.92	77.13
PCA preprocessed	Pack 1	100	100	100
	Pack 2	99.32	99.66	98.98
	Pack 3	92.83	92.49	93.86
	Pack 4	92.83	92.83	93.86
	Pack 5	69.28	48.12	77.13
LDA preprocessed	Pack 1	100	100	100
	Pack 2	99.66	100	98.63
	Pack 3	97.27	97.27	96.93
	Pack 4	93.17	95.90	94.88
	Pack 5	70.31	53.92	77.13
LDA after PCA preprocessed	Pack 1	100	100	100
	Pack 2	99.66	99.66	99.66
	Pack 3	92.83	92.49	93.86
	Pack 4	97.27	97.27	96.93
	Pack 5	69.28	48.12	77.13
PCA after LDA preprocessed	Pack 1	100	100	99.66
	Pack 2	99.32	99.32	98.98
	Pack 3	90.10	51.19	90.44
	Pack 4	92.83	92.83	93.86
	Pack 5	69.28	48.12	77.13

The classification accuracies of the proposed approach for each feature pack of the channel2 test dataset.

TABLE 9. The CCR comparison for the channel1 train dataset.

Pack number	Method	SVM RBF	SVM POLYNOMIAL	KNN
Pack1	our method	98.88	99.25	98.88
	Paranjape et al. [11]	82.40±7.95	82.77±5.52	76.40±7.71
Pack2	our method	99.25	99.25	98.88
	Paranjape et al. [11]	81.65±6.36	79.78±9.12	76.40±7.95
Pack3	our method	62.69	51.49	58.21
	Paranjape et al. [11]	81.65±9.67	82.02±5.77	77.90±7.83

Comparison of the classification accuracy between the proposed method and [11], for not-preprocessed features of the training dataset of channel1.

TABLE 10. The CCR comparison for the channel2 train dataset.

Pack number	Method	SVM RBF	SVM POLYNOMIAL	KNN
Pack3	our method	84.70	85.07	83.96
	Paranjape et al. [11]	82.77±5.22	83.15±9.39	80.15±6.28
Pack4	our method	84.70	85.45	83.96
	Paranjape et al. [11]	81.27±8.04	76.78±12.15	79.78±6.25
Pack5	our method	57.09	42.91	67.16
	Paranjape et al. [11]	76.78±10.03	71.54±6.96	74.16±11.08

Comparison of the classification accuracy between the proposed method and [11], for not-preprocessed features of the training dataset of channel2.

TABLE 11. Performance measures comparison.

		ACCURACY	SENSITIVITY	SPECIFICITY	F-MEASURE	KAPPA
our method	Train dataset	0.9925	0.9887	0.9963	0.9925	0.9851
Paranjape et al. [11]	Train dataset	0.8258	0.7891	0.8717	0.8345	0.6518
our method	Test dataset	0.9983	0.9966	1.0000	0.9983	0.9966
Paranjape et al. [11]	Test dataset	0.9454	0.9226	0.9710	0.9470	0.8908

Comparison of the best results of the proposed method and [11] for various performance measures, via not-preprocessed features of the train and test datasets.

5- In addition to the method described in [11], the feature packs are processed using PCA, LDA, and their composition to investigate the effect of feature preprocessing.

6- Three classifiers receive the features in five formats: not-preprocessed, PCA, LDA, LDA after PCA, and PCA after LDA preprocessed. According to [11], the implemented

TABLE 12. The CCR comparison with the other proposed methods.

Author	Year	# of Features	# of Channels	Features	Classifier	CCR
Mensh et al. [48]	2004	4	4	SCP and Gamma-band power	SCP and Multi-taper	88.70%
Sun et al. [13]	2005	7	6	SCP and spectral centroid	Bayesian	90.44%
Wang et al. [65]	2006	4	2	Beta band energy of Wavelet Packet Transform	Neural Networks	91.47%
Yi et al. [14]	2008	2	2	Kolmogorov and C0 Complexity Discriminant	Fisher Linear	90.30%
Kayikcioglu et al. [15]	2010	2	1	Polynomial fitting	K Nearest Neighbor	92.15%
Hu et al. [16]	2011	10	6	mean and energy of Wavelet Packet Decomposition	K Nearest Neighbor	90.10%
Duan et al. [17]	2014	18	2	LDA after PCA	Voting Based Extreme Learning Machine	93.52%
Nguyen et al. [18]	2015	6	6	Wavelet coefficients	Interval type-2 Fuzzy Logic System	90.10%
Duan et al. [20]	2016	1	2	PCA and LDA	Multilayer Extreme Learning Machine	94.20%
Göksu [68]	2018	42	6	Log Energy Entropy of Wavelet Packet Analysis	Multilayer Perceptron	92.83%
Hou et al. [19]	2018	1	3	Polynomial fitting	Voting Support Vector Machines	94.50%
Paranjape et al. [11]	2019	5	2	Peak value, instant at which peak occurs, centroid, equivalent width, and mean square abscissa, via cross-correlation	SVM RBF, SVM polynomial, and K Nearest Neighbor	95.54%
Annaby et al. [12]	2021	6	6	Symmetric-Laplacian graph Fourier transform, LDA after PCA, fitting polynomial coefficients	Online Sequential Extreme Learning Machine	96.58%
our proposed method	2022	5	2	Peak value, instant at which peak occurs, centroid, equivalent width, and mean square abscissa, via spectral correlation	SVM RBF, SVM polynomial, and K Nearest Neighbor	99.83%

Comparison of the current EEG-based motor imagery categorization methods for the BCI Competition 2003 dataset Ia.

classifiers include SVM RBF, SVM polynomial, and K-Nearest Neighbor, and 10-fold cross-validation was used to analyze the accuracy.

The method's flowchart is shown in figure 4.

The classification accuracy for the not-preprocessed features from the training and testing datasets is shown in tables 3 and 4. The classifiers in the first research are fed with all of the extracted features from both channels, and in the second study, the classification accuracy per each pack of features is evaluated. It has been observed that in general, the performance of the packs with more features is superior. The highest performance was 99.83% and the lowest was 49.81% CCR.

Additionally, we looked at the performance of the classifiers individually for each pack of features extracted from each channel. Tables 5 to 8 illustrate the performance of this analysis, with the best performance being 100% CCR for pack1 of channel 2 of the training dataset across all classifiers and the worst performance being 33.21% CCR for the PCA-preprocessed pack3 of the training dataset via SVM Polynomial classifier. The classification accuracy is typically decreased by lonely channel feature preprocessing. This is the result of classifying the data using only the remaining features after removing the features from the second channel and also eliminating the distinguishing features through preprocessing techniques.

Tables 9 and 10 and Figures 5 and 6 compare the proposed method's accuracy to that of [11] for features that have not been preprocessed, to have a fair comparison. As can be observed, choosing the appropriate method at the correlation block by taking into account the inherent characteristics of SCP EEG signals, considerably improved classification performance. The Spectral Correlation Function (SCF) reveals the fundamental correlation between signals, generating important information for BCI-oriented EEG classification. Table 11 presents the comparison of the best results for the proposed method and [11] for various performance measures, via not-preprocessed features of the train and test datasets. The BCI Competition 2003 dataset Ia is compared in Table 12 in terms of the number and types of features, the number of channels, the types of features, and classifiers used.

V. CONCLUSION

In this paper, the applicability of cyclostationary analysis at EEG-based Brain-Computer Interfaces (BCIs) was investigated. Following our previous research, we studied the cyclostationarity for Slow Cortical Potential (SCP)

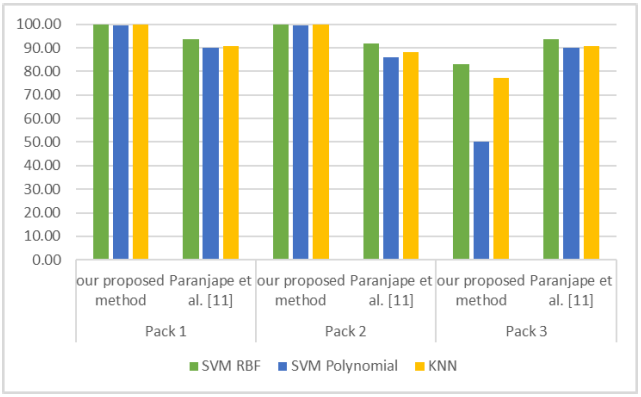

FIGURE 5. Comparison of the classification accuracy between the proposed method and [11], for not-preprocessed features of the test dataset of channel1.

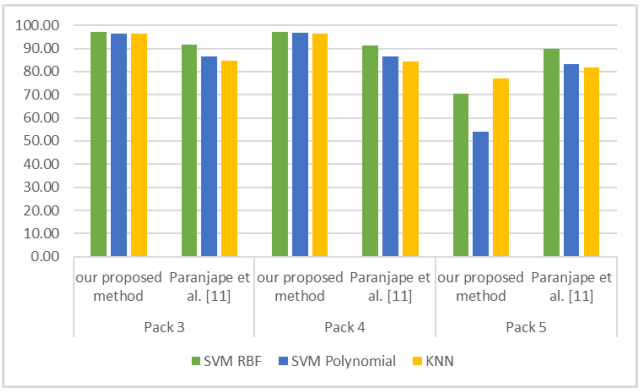

FIGURE 6. Comparison of the classification accuracy between the proposed method and [11], for not-preprocessed features of the test dataset of channel2.

EEG signals and the findings support it. By choosing the appropriate method at the correlation block of the feature extraction phase, the classification performance was greatly improved. The hidden periodicities and fundamental correlation between SCP signals are revealed by the Spectral Correlation Function (SCF), producing significant features for BCI-oriented EEG classification. We also studied the influence of feature preprocessing by Linear Discriminate Analysis (LDA), Principal Component Analysis (PCA), and their combination at the Correct Classification Rate (CCR). Our finding on the dataset Ia from the BCI Competition 2003 showed that the generated features may correctly classify the SCP EEG signals for BCI applications.

REFERENCES

[1] A. Kawala-Sterniuk, N. Browarska, A. Al-Bakri, M. Pelc, J. Zygarlicki, M. Sidikova, R. Martinek, and E. J. Gorzelanczyk, "Summary of over fifty years with brain-computer interfaces—A review," *Brain Sci.*, vol. 11, no. 1, p. 43, Jan. 2021, doi: 10.3390/brainsci11010043.

[2] X. Gao, Y. Wang, X. Chen, and S. Gao, "Interface, interaction, and intelligence in generalized brain–computer interfaces," *Trends Cogn. Sci.*, vol. 25, no. 8, pp. 671–684, Aug. 2021, doi: 10.1016/j.tics.2021.04.003.

[3] A. D. Gerson, L. C. Parra, and P. Sajda, "Cortically coupled computer vision for rapid image search," *IEEE Trans. Neural Syst. Rehabil. Eng.*, vol. 14, no. 2, pp. 174–179, Jun. 2006.

[4] E. Netzer and A. B. Geva, "Human-in-the-loop active learning via brain computer interface," *Ann. Math. Artif. Intell.*, vol. 88, nos. 11–12, pp. 1191–1205, Dec. 2020.

[5] S. Saproo, J. Faller, V. Shih, P. Sajda, N. R. Waytowich, A. Bohannon, V. J. Lawhern, B. J. Lance, and D. Jangraw, "Cortically coupled computing: A new paradigm for synergistic human-machine interaction," *Computer*, vol. 49, no. 9, pp. 60–68, Sep. 2016.

[6] S. Lees, N. Dayan, H. Cecotti, P. McCullagh, L. Maguire, F. Lotte, and D. Coyle, "A review of rapid serial visual presentation-based brain–computer interface," *J. Neural Eng.*, vol. 15, no. 2, 2018, Art. no. 021001.

[7] A. Al-Saegh, S. A. Dawwd, and J. M. Abdul-Jabbar, "Deep learning for motor imagery EEG-based classification: A review," *Biomed. Signal Process. Control*, vol. 63, Jan. 2021, Art. no. 102172.

[8] M. Z. Baig, N. Aslam, H. P. H. Shum, and L. Zhang, "Differential evolution algorithm as a tool for optimal feature subset selection in motor imagery EEG," *Expert Syst. Appl.*, vol. 90, pp. 184–195, Dec. 2017, doi: 10.1016/j.eswa.2017.07.033.

[9] N. Padfield, J. Zabalza, H. Zhao, V. Masero, and J. Ren, "EEG-based brain-computer interfaces using motor-imagery: Techniques and challenges," *Sensors*, vol. 19, no. 6, p. 1423, Mar. 2019, doi: 10.3390/s19061423.

[10] F. Li, F. He, F. Wang, D. Zhang, Y. Xia, and X. Li, "A novel simplified convolutional neural network classification algorithm of motor imagery EEG signals based on deep learning," *Appl. Sci.*, vol. 10, no. 5, p. 1605, Feb. 2020, doi: 10.3390/app10051605.

[11] P. N. Paranjape, M. M. Dhabu, P. S. Deshpande, and A. M. Kekre, "Cross-correlation aided ensemble of classifiers for BCI oriented EEG study," *IEEE Access*, vol. 7, pp. 11985–11996, 2019.

[12] M. H. Annaby, M. H. Said, A. M. Eldeib, and M. A. Rushdi, "EEG-based motor imagery classification using digraph Fourier transforms and extreme learning machines," *Biomed. Signal Process. Control*, vol. 69, Aug. 2021, Art. no. 102831.

[13] S. Sun and C. Zhang, "Assessing features for electroencephalographic signal categorization," in *Proc. IEEE Int. Conf. Acoust., Speech, Signal Process. (ICASSP)*, vol. 5, Mar. 2005, pp. v/417–v/420.

[14] L. Yi, F. Yingle, and T. Qinye, "EEG feature detection and classification algorithm in brain-computation interface," in *Proc. 3rd IEEE Conf. Ind. Electron. Appl.*, Jun. 2008, pp. 1403–1407.

[15] T. Kayikcioglu and O. Aydemir, "A polynomial fitting and k-NN based approach for improving classification of motor imagery BCI data," *Pattern Recognit. Lett.*, vol. 31, no. 11, pp. 1207–1215, Aug. 2010.

[16] D. Hu, W. Li, and X. Chen, "Feature extraction of motor imagery EEG signals based on wavelet packet decomposition," in *Proc. IEEE/ICME Int. Conf. Complex Med. Eng.*, Harbin, China, May 2011, pp. 694–697.

[17] L. Duan, H. Zhong, J. Miao, Z. Yang, W. Ma, and X. Zhang, "A voting optimized strategy based on ELM for improving classification of motor imagery BCI data," *Cogn. Comput.*, vol. 6, no. 3, pp. 477–483, Sep. 2014, doi: 10.1007/s12559-014-9264-1.

[18] T. Nguyen, A. Khosravi, D. Creighton, and S. Nahavandi, "EEG signal classification for BCI applications by wavelets and interval type-2 fuzzy logic systems," *Expert Syst. Appl.*, vol. 42, no. 9, pp. 4370–4380, Jun. 2015.

[19] H.-R. Hou, Q.-H. Meng, M. Zeng, and B. Sun, "Improving classification of slow cortical potential signals for BCI systems with polynomial fitting and voting support vector machine," *IEEE Signal Process. Lett.*, vol. 25, no. 2, pp. 283–287, Feb. 2018.

[20] L. Duan, M. Bao, J. Miao, Y. Xu, and J. Chen, "Classification based on multilayer extreme learning machine for motor imagery task from EEG signals," *Proc. Comput. Sci.*, vol. 88, pp. 176–184, Jan. 2016.

[21] B. Sorger and R. Goebel, "Real-time fMRI for brain-computer interfacing," in *Handbook of Clinical Neurology*. Elsevier, vol. 168, 2020, pp. 289–302. [Online]. Available: https://cris.maastrichtuniversity.nl/en/publications/real-time-fmri-for-brain-computer-interfacing, doi: 10.1016/B978-0-444-63934-9.00021-4.

[22] R. A. Ramadan and A. V. Vasilakos, "Brain computer interface: Control signals review," *Neurocomputing*, vol. 223, pp. 26–44, Feb. 2017.

[23] K.-S. Hong, M. J. Khan, and M. J. Hong, "Feature extraction and classification methods for hybrid fNIRS-EEG brain-computer interfaces," *Frontiers Hum. Neurosci.*, vol. 12, p. 246, Jun. 2018.

[24] B. K. Min, M. J. Marzelli, and S. S. Yoo, "Neuroimaging-based approaches in the brain–computer interface," *Trends Biotechnol.*, vol. 28, pp. 552–560, Nov. 2010.
[25] G. Schalk and E. C. Leuthardt, "Brain-computer interfaces using electrocorticographic signals," *IEEE Rev. Biomed. Eng.*, vol. 4, pp. 140–154, 2011.
[26] K.-S. Hong and M. J. Khan, "Hybrid brain–computer interface techniques for improved classification accuracy and increased number of commands: A review," *Frontiers Neurorobot.*, vol. 11, p. 35, Jul. 2017, doi: 10.3389/fnbot.2017.00035.
[27] Y. Kwak, W.-J. Song, and S.-E. Kim, "FGANet: FNIRS-guided attention network for hybrid EEG-fNIRS brain-computer interfaces," *IEEE Trans. Neural Syst. Rehabil. Eng.*, vol. 30, pp. 329–339, 2022.
[28] *Intro to Brain Computer Interface*. [Online]. Available: http://learn.neurotechedu.com/introtobci/#what-are–the-types-of-bcis
[29] M. Bachmann, L. Päeske, K. Kalev, K. Aarma, A. Lehtmets, P. Ööpik, J. Lass, and H. Hinrikus, "Methods for classifying depression in single channel EEG using linear and nonlinear signal analysis," *Comput. Methods Programs Biomed.*, vol. 155, pp. 11–17, Mar. 2018, doi: 10.1016/j.cmpb.2017.11.023.
[30] L. Tylová, J. Kukal, V. Hubata-Vacek, and O. Vyšata, "Unbiased estimation of permutation entropy in EEG analysis for Alzheimer's disease classification," *Biomed. Signal Process. Control*, vol. 39, pp. 424–430, Jan. 2018.
[31] A. Bhattacharyya and R. B. Pachori, "A multivariate approach for patient-specific EEG seizure detection using empirical wavelet transform," *IEEE Trans. Biomed. Eng.*, vol. 64, no. 9, pp. 2003–2015, Sep. 2017, doi: 10.1109/TBME.2017.2650259.
[32] M. Aldayel, M. Ykhlef, and A. Al-Nafjan, "Deep learning for EEG-based preference classification in neuromarketing," *Appl. Sci.*, vol. 10, no. 4, p. 1525, Feb. 2020, doi: 10.3390/app10041525.
[33] J. Heo and G. Yoon, "EEG studies on physical discomforts induced by virtual reality gaming," *J. Electr. Eng. Technol.*, vol. 15, no. 3, pp. 1323–1329, May 2020, doi: 10.1007/s42835-020-00373-1.
[34] J. N. Mak and J. R. Wolpaw, "Clinical applications of brain-computer interfaces: Current state and future prospects," *IEEE Rev. Biomed. Eng.*, vol. 2, pp. 187–199, 2009, doi: 10.1109/RBME.2009.2035356.
[35] L. Kramer, C. Sander, K. Bertsch, D. M. Gescher, S. Cackowski, U. Hegerl, and S. C. Herpertz, "EEG-vigilance regulation in borderline personality disorder," *Int. J. Psychophysiol.*, vol. 139, pp. 10–17, May 2019.
[36] Z. Liu, J. Sun, Y. Zhang, and P. Rolfe, "Sleep staging from the EEG signal using multi-domain feature extraction," *Biomed. Signal Process. Control*, vol. 30, pp. 86–97, Sep. 2016.
[37] A. A. Lins, J. M. de Oliveira, J. J. P. C. Rodrigues, and V. H. C. de Albuquerque, "Robot-assisted therapy for rehabilitation of children with cerebral palsy—A complementary and alternative approach," *Comput. Hum. Behav.*, vol. 100, pp. 152–167, Nov. 2019.
[38] S. N. Abdulkader, A. Atia, and M.-S.-M. Mostafa, "Brain computer interfacing: Applications and challenges," *Egyptian Informat. J.*, vol. 16, no. 2, pp. 213–230, Jul. 2015, doi: 10.1016/j.eij.2015.06.002.
[39] Z. A. A. Alyasseri, A. T. Khader, M. A. Al-Betar, and O. A. Alomari, "Person identification using EEG channel selection with hybrid flower pollination algorithm," *Pattern Recognit.*, vol. 105, Sep. 2020, Art. no. 107393, doi: 10.1016/j.patcog.2020.107393.
[40] Z. A. A. Alyasseri, A. T. Khader, M. A. Al-Betar, J. P. Papa, and O. A. Alomari, "EEG-based person authentication using multi-objective flower pollination algorithm," in *Proc. IEEE Congr. Evol. Comput. (CEC)*, Jul. 2018, pp. 1–8, doi: 10.1109/CEC.2018.8477895.
[41] Z. A. A. Alyasseri, A. T. Khader, M. A. Al-Betar, J. P. Papa, O. A. Alomari, and S. N. Makhadme, "An efficient optimization technique of EEG decomposition for user authentication system," in *Proc. 2nd Int. Conf. BioSignal Anal., Process. Syst. (ICBAPS)*, Jul. 2018, pp. 1–6, doi: 10.1109/ICBAPS.2018.8527404.
[42] A. Czeszumski, S. Eustergerling, A. Lang, D. Menrath, M. Gerstenberger, S. Schuberth, F. Schreiber, Z. Z. Rendon, and P. König, "Hyperscanning: A valid method to study neural inter-brain underpinnings of social interaction," *Frontiers Hum. Neurosci.*, vol. 14, p. 39, Feb. 2020, doi: 10.3389/fnhum.2020.00039.
[43] F. H. Guenther, J. S. Brumberg, E. J. Wright, A. Nieto-Castanon, J. A. Tourville, M. Panko, R. Law, S. A. Siebert, J. L. Bartels, D. S. Andreasen, P. Ehirim, H. Mao, and P. R. Kennedy, "A wireless brain-machine interface for real-time speech synthesis," *PLoS ONE*, vol. 4, no. 12, 2009, Art. no. e8218.
[44] C. Cooney, R. Folli, and D. Coyle, "Neurolinguistics research advancing development of a direct-speech brain-computer interface," *iScience*, vol. 8, pp. 103–125, Oct. 2018.
[45] Q. Rabbani, G. Milsap, and N. E. Crone, "The potential for a speech brain–computer interface using chronic electrocorticography," *Neurotherapeutics*, vol. 16, no. 1, pp. 144–165, Jan. 2019.
[46] F. Velasco-Álvarez, Á. Fernández-Rodríguez, and R. Ron-Angevin, "Brain-computer interface (BCI)-generated speech to control domotic devices," *Neurocomputing*, vol. 509, pp. 121–136, Oct. 2022, doi: 10.1016/j.neucom.2022.08.068.
[47] T. K. Reddy and L. Behera, "Driver drowsiness detection: An approach based on intelligent brain–computer interfaces," *IEEE Syst., Man, Cybern. Mag.*, vol. 8, no. 1, pp. 16–28, Jan. 2022.
[48] B. D. Mensh, J. Werfel, and H. S. Seung, "BCI competition 2003-data set IA: Combining gamma-band power with slow cortical potentials to improve single-trial classification of electroencephalographic signals," *IEEE Trans. Biomed. Eng.*, vol. 51, no. 6, pp. 1052–1056, Jun. 2004.
[49] S. Bengio, "HMM and IOHMM modeling of EEG rhythms for asynchronous BCI systems," in *Proc. Eur. Symp. Artif. Neural Netw. (ESANN)*, 2004, pp. 199–204.
[50] N. Shi, L. Wang, Y. Chen, X. Yan, C. Yang, Y. Wang, and X. Gao, "Steady-state visual evoked potential (SSVEP)-based brain–computer interface (BCI) of Chinese speller for a patient with amyotrophic lateral sclerosis: A case report," *J. Neurorestoratol.*, vol. 8, no. 1, pp. 40–52, Mar. 2020, doi: 10.26599/JNR.2020.9040003.
[51] R. Bian, L. Meng, and D. Wu, "SSVEP-based brain-computer interfaces are vulnerable to square wave attacks," *Sci. China Inf. Sci.*, vol. 65, pp. 140406:1–140406:13, Apr. 2022, doi: 10.1007/s11432-022-3440-5.
[52] F. Guo, B. Hong, X. Gao, and S. Gao, "A brain–computer interface using motion-onset visual evoked potential," *J. Neural Eng.*, vol. 5, no. 4, pp. 477–485, Dec. 2008, doi: 10.1088/1741-2560/5/4/011.
[53] E. Donchin, K. M. Spencer, and R. Wijesinghe, "The mental prosthesis: Assessing the speed of a P300-based brain-computer interface," *IEEE Trans. Rehabil. Eng.*, vol. 8, no. 2, pp. 174–179, Jun. 2000.
[54] U. Hoffmann, J.-M. Vesin, T. Ebrahimi, and K. Diserens, "An efficient P300-based brain–computer interface for disabled subjects," *J. Neurosci. Methods*, vol. 167, no. 1, pp. 115–125, Jan. 2008.
[55] J. Pan, X. Chen, N. Ban, J. He, J. Chen, and H. Huang, "Advances in P300 brain–computer interface spellers: Toward paradigm design and performance evaluation," *Frontiers Hum. Neurosci.*, vol. 16, pp. 1–13, Dec. 2022, doi: 10.3389/fnhum.2022.1077717.
[56] D. S. Ramanathan, L. Guo, T. Gulati, G. Davidson, A. K. Hishinuma, S.-J. Won, R. T. Knight, E. F. Chang, R. A. Swanson, and K. Ganguly, "Low-frequency cortical activity is a neuromodulatory target that tracks recovery after stroke," *Nature Med.*, vol. 24, no. 8, pp. 1257–1267, Aug. 2018.
[57] B. J. He, "Robust, transient neural dynamics during conscious perception," *Trends Cogn. Sci.*, vol. 22, no. 7, pp. 563–565, Jul. 2018.
[58] M. Halgren, D. Fabó, I. Ulbert, J. R. Madsen, L. Erőss, W. K. Doyle, O. Devinsky, D. Schomer, S. S. Cash, and E. Halgren, "Superficial slow rhythms integrate cortical processing in humans," *Sci. Rep.*, vol. 8, no. 1, p. 2055, Feb. 2018.
[59] G. P. Krishnan, O. C. González, and M. Bazhenov, "Origin of slow spontaneous resting-state neuronal fluctuations in brain networks," *Proc. Nat. Acad. Sci. USA*, vol. 115, no. 26, pp. 6858–6863, 2018.
[60] H. Heinrich, H. Gevensleben, F. J. Freisleder, G. H. Moll, and A. Rothenberger, "Training of slow cortical potentials in attention-deficit/hyperactivity disorder: Evidence for positive behavioral and neurophysiological effects," *Biol. Psychiatry*, vol. 55, no. 7, pp. 772–775, Apr. 2004.
[61] U. Strehl, U. Leins, G. Goth, C. Klinger, T. Hinterberger, and N. Birbaumer, "Self-regulation of slow cortical potentials: A new treatment for children with attention-deficit/hyperactivity disorder," *Pediatrics*, vol. 118, no. 5, pp. 1530–1540, 2006.
[62] H. Christiansen, V. Reh, M. H. Schmidt, and W. Rief, "Slow cortical potential neurofeedback and self-management training in outpatient care for children with ADHD: Study protocol and first preliminary results of a randomized controlled trial," *Frontiers Hum. Neurosci.*, vol. 8, p. 943, Nov. 2014.

[63] K. Mayer, F. Blume, S. N. Wyckoff, L. L. Brokmeier, and U. Strehl, "Neurofeedback of slow cortical potentials as a treatment for adults with attention deficit-/hyperactivity disorder," *Clin. Neurophysiol.*, vol. 127, no. 2, pp. 1374–1386, Feb. 2016.
[64] B. Blankertz, K.-R. Müller, G. Curio, T. M. Vaughan, G. Schalk, J. R. Wolpaw, A. Schlogl, C. Neuper, G. Pfurtscheller, T. Hinterberger, M. Schroder, and N. Birbaumer, "The BCI competition 2003: Progress and perspectives in detection and discrimination of EEG single trials," *IEEE Trans. Biomed. Eng.*, vol. 51, no. 6, pp. 1044–1051, Jun. 2004.
[65] B. Wang, L. Jun, J. Bai, L. Peng, G. Li, and Y. Li, "EEG recognition based on multiple types of information by using wavelet packet transform and neural networks," in *Proc. IEEE Eng. Med. Biol. 27th Annu. Conf.*, Shanghai, China, Sep. 2005, pp. 5377–5380.
[66] L. Yi and F. Yingle, "Complexity measure applied to the analysis EEG signals," in *Proc. IEEE Eng. Med. Biol. 27th Annu. Conf. (IEEE-EMBS)*, Jan. 2005, pp. 4610–4613.
[67] L. Duan, Q. Zhang, Z. Yang, and J. Miao, "Research on heuristic feature extraction and classification of EEG signal based on BCI data set," *Res. J. Appl. Sci., Eng. Technol.*, vol. 5, no. 3, pp. 1008–1014, Jan. 2013.
[68] H. Göksu, "BCI oriented EEG analysis using log energy entropy of wavelet packets," *Biomed. Signal Process. Control*, vol. 44, pp. 101–109, Jul. 2018.
[69] S. Kumar, T. K. Reddy, V. Arora, and L. Behera, "Formulating divergence framework for multiclass motor imagery EEG brain computer interface," in *Proc. IEEE Int. Conf. Acoust., Speech Signal Process. (ICASSP)*, May 2020, pp. 1344–1348.
[70] K. Sadatnejad and F. Lotte, "Riemannian channel selection for BCI with between-session non-stationarity reduction capabilities," *IEEE Trans. Neural Syst. Rehabil. Eng.*, vol. 30, pp. 1158–1171, 2022.
[71] S. Mihandoost and M. C. Amirani, "Cyclic spectral analysis of electrocardiogram signals based on GARCH model," *Biomed. Signal Process. Control*, vol. 31, pp. 79–88, Jan. 2017.
[72] S. Mihandoost and M. C. Amirani, "EEG signal analysis using spectral correlation function & GARCH model," *Signal, Image Video Process.*, vol. 9, pp. 1461–1472, Jan. 2014, doi: 10.1007/s11760-013-0600-9.
[73] W. A. Gardner, "The spectral correlation theory of cyclostationary time-series," *Signal Process.*, vol. 11, no. 1, pp. 13–36, 1986.
[74] W. Gardner, "Measurement of spectral correlation," *IEEE Trans. Acoust., Speech, Signal Process.*, vol. ASSP-34, no. 5, pp. 1111–1123, Oct. 1986.
[75] W. A. Gardner, *Statistical Spectral Analysis: A Nonprobabilistic Theory*. Englewood Cliffs, NJ, USA: Prentice-Hall, 1987.
[76] W. Gardner, "Spectral correlation of modulated signals: Part I—Analog modulation," *IEEE Trans. Commun.*, vol. COM-35, no. 6, pp. 584–594, Jun. 1987.
[77] W. Gardner, W. Brown, and C.-K. Chen, "Spectral correlation of modulated signals: Part II—Digital modulation," *IEEE Trans. Commun.*, vol. COM-35, no. 6, pp. 595–601, Jun. 1987.
[78] R. S. Roberts, W. A. Brown, and H. H. Loomis, "Computationally efficient algorithms for cyclic spectral analysis," *IEEE Signal Process. Mag.*, vol. 8, no. 2, pp. 38–49, Apr. 1991.
[79] M. C. Amirani, "Modulation classification of communication signals using cyclic spectral analyzer," M.S. dissertation, Dept. Elect. Eng., Iran Univ. Sci. Technol., Tehran, Iran, 1998.
[80] M. C. Amirani and A. A. B. Shirazi, "Evaluation of the texture analysis using spectral correlation function," *Fundamenta Informaticae*, vol. 95, pp. 245–262, Jan. 2009, doi: 10.3233/FI-2009-149.
[81] S. Mihandoost and M. Chehel Amirani, "Two-dimensional strip spectral correlation algorithm to fast estimation of 2D-cyclic spectral function for texture analysis," *Multidimensional Syst. Signal Process.*, vol. 29, no. 3, pp. 1119–1134, Jul. 2018, doi: 10.1007/s11045-017-0492-x.
[82] N. Panahi, M. G. Shayesteh, S. Mihandoost, and B. Z. Varghahan, "Recognition of different datasets using PCA, LDA, and various classifiers," in *Proc. 5th Int. Conf. Appl. Inf. Commun. Technol. (AICT)*, Oct. 2011, pp. 1–5.
[83] H. Hou, B. Sun, and Q. Meng, "Slow cortical potential signal classification using concave–convex feature," *J. Neurosci. Methods*, vol. 324, Aug. 2019, Art. no. 108303.
[84] Y.-C. Lim, J.-H. Lee, C. K. Chen, and R.-H. Yang, "A weighted least squares algorithm for quasi-equiripple FIR and IIR digital filter design," *IEEE Trans. Signal Process.*, vol. 40, no. 3, pp. 551–558, Mar. 1992.
[85] R. Crochiere and L. Rabiner, *Multirate Digital Signal Processing*. Englewood Cliffs, NJ, USA: Prentice-Hall, 1983.

NAZILA PANAHI received the B.Sc. degree in telecommunication engineering from Islamic Azad University, Urmia Branch, Urmia, Iran, in 2008, and the M.Sc. degree in telecommunication engineering from Urmia University, Urmia, in 2012, where she is currently pursuing the Ph.D. degree.

Her research interests include signal processing, pattern recognition, watermarking, and biometrics.

MEHDI CHEHEL AMIRANI received the B.Sc. degree in electronic engineering from Urmia University, Urmia, Iran, in 1993, and the M.Sc. and Ph.D. degrees in communication engineering from the Iran University of Science and Technology (IUST), Tehran, Iran, in 1998 and 2009, respectively.

He is currently a Professor in communication with Urmia University. His research interests include pattern recognition, digital signal processing, and secure communication.

MORTEZA VALIZADEH received the M.Sc. and Ph.D. degrees in electronic engineering from Tarbiat Modares University, Tehran, Iran, in 2008 and 2012, respectively.

He is currently an Associate Professor in communication with Urmia University, Urmia, Iran. His research interests include image processing, medical signal analysis, machine vision, and deep learning.